Why is the measured maximum lift in wind tunnels dependent on the measurement method?

Olsen, A. S.; Sørensen, N. N.; Bak, C.; Gaunaa, M.; Mikkelsen, R.; Fischer, A.; Beckerlee, J.; Ildvedsen, S.

Published in:
Journal of Physics: Conference Series

Link to article, DOI:
10.1088/1742-6596/1618/3/032040

Publication date:
2020

Document Version
Publisher's PDF, also known as Version of record

Why is the measured maximum lift in wind tunnels dependent on the measurement method?

Why is the measured maximum lift in wind tunnels dependent on the measurement method?

A S Olsen[1], N N Sørensen[1], C Bak[1], M Gaunaa[1], R Mikkelsen[2], A Fischer[1], J Beckerlee[1], S Ildvedsen[1]

[1] Department of Wind Energy, DTU, Frederiksborgvej 399, Building 114, 4000 Roskilde, Denmark

[2] Department of Wind Energy, DTU, Niels Koppels Allé, Building 403, 2800 Kgs. Lyngby, Denmark

Author contact email: sols@dtu.dk

Abstract. The present study investigates the differences in the predicted lift for a wind tunnel model from either surface pressures or side wall pressures. The investigated model is the NACA63-418 tested in the Poul la Cour tunnel. The measurements are compared with previous conducted wind tunnel campaigns for a Reynolds number of 3E6. The 3D CFD model of the wind tunnel will be used for investigating details of the flow mechanisms, and to validate assumptions and findings from the experimental data. The CFD simulations show that when the flow is attached the lift based on the side wall pressures results in almost the same lift as calculated from the surface pressures. Around the maximum lift and in the stalled region the flow is not anymore 2D. For the NACA63-418 airfoil the lift based on the side wall pressures are generally highest. The CFD simulations confirm that the method used to predict the lift from the limited side wall pressure strips in the wind tunnel is applicable.

1. Introduction

For most wind tunnels, it is common practice to have redundant measurement methods for the loads on the airfoil models. In order for these methods to be truly redundant, they need to give the same results. However, this is not always the case and it is often seen that the maximum lift determined from tunnel wall pressures and the airfoil surface pressures differ and differences are especially seen around and after maximum lift. This is challenging, as an accurate prediction of the maximum lift is important for load calculations of wind turbines and prediction of stall margins.

The basic assumption of the wind tunnel airfoil testing is that the flow is two-dimensional. This is of course violated in the stall region, where the flow separates resulting in highly 3D flow over the wind tunnel model.

Nevertheless, the data from the stall region are being used and therefore it is of interest to know the mechanisms in the tests and what can be considered the best representation of the lift in the stalled region.

One characteristic of the flow in the stalled region is the formation of stall cells. The characteristics of stall cells have been examined in [1] and [2]. The stall cells influences the separation on the model

and the extent of the separation changes along the span of the model (3D flow), hence the lift on the different spanwise sections differ. This spanwise variation influences the measurements of the lift. If the lift is based on surface pressures it is common practice to stagger the pressure orifices in a relative narrow spanwise band. This band can in principle be placed at any spanwise position, but is often located around midspan in order to avoid the influence from the end walls. Hence, the lift predicted by the surface pressures can be considered a relatively local prediction. This is in contrast to the lift predicted from the pressures measured at the side walls. This lift is an average value as the pressures measured at the walls dependent on the flow over the entire span of the model.

The objectives of the present study is to evaluate and compare the measured lift coefficient from the airfoil surface pressures and the tunnel wall pressures for an airfoil model in a wind tunnel. Especially, the differences seen around maximum lift and in the stalled region are evaluated. The 3D CFD model of the wind tunnel will be used for investigating details of the flow mechanisms, and to validate assumptions and findings from the experimental data.

Figure 1. The NACA63-418 wind tunnel model mounted in the PLCT. The wake rake is seen in the back supported by the two vertical struts.

2. Methodology

2.1. Wind tunnel

Lift polars for the NACA63-418 airfoil at a Reynolds number of 3E6 are measured in the Poul la Cour tunnel (PLCT) at DTU Risø campus. The test section is 2m high and 3m wide, and the 2D airfoil section is placed vertically in the tunnel. Along each sidewall, the wall pressures are measured at 64 orifices distributed in two bands with 48 and 16 orifices, respectively. Each band span 2.85m upstream and downstream of the turntable centre and is placed 0.27m on either side of the horizontal centre line.

The pressures are measured by six ScaniValve MPS4264 pressure scanners with 64 channels each. The sensitivity ranges from 1 kPa (4 inch H_2O) to 69 kPa (10 PSI). In addition to the scanners a number of sensors are measuring the state of the flow (i.e. the temperature, the relative humidity, and the barometric pressure), the angle of attack of the model and the wake rake position.

The data acquisition (DAQ) system is based upon cRIO from National Instruments and a DTU in-house made LabView program.

The airfoil model has a 1m chord, 2m span, giving an aspect ratio of 2 and a chord to tunnel-width ratio of 3. 100 pressure orifices are staggered around the midspan. Figure 1 shows the model in the PLCT.

2.2. CFD

The contraction, the test section and the diffusor of the PLCT is modelled in the DTU in-house CFD code EllipSys3D [3]-[5]. The EllipSys3D solver, uses the time true IDDES model based on the $k-\omega$ SST model, along with the $\gamma - Re_\Theta$ correlation based transition model.

The airfoil lift is evaluated based on viscous stresses and pressures on the airfoil model and on the tunnel walls, allowing for direct comparisons between calculations and measurements. The details of the CFD simulations are found in the accompanied paper [6].

The CFD simulations were originally targeted at low angle of attacks including only a few deep stall angles. Here the CFD results are mainly used to explain the qualitative 3D flow characteristics, due to the well know inaccuracy of the RANSE CFD in stall. The lift and drag have though been included for completeness.

2.3. C_l calculation

The C_l is calculated by two different methods, either by an integration of the surface pressures on the airfoil or by an integration of the pressure footprint on the tunnel side walls.

A simplified expression for the pressure footprint from the airfoil model on the tunnel side walls can be derived using cascade singularity elements from potential theory [7]:

$$\frac{\Delta C_p}{C_l} = \frac{c}{H}\frac{1}{\cosh\left(\pi\frac{x}{H}\right)} \tag{1}$$

Where ΔC_p is the pressure difference coefficient between the pressures on the two side walls, c is the chord, H is the tunnel width and C_l is the lift coefficient, x is the streamwise coordinate (positive downstream) measured from the point on the aerofoil where the aerodynamic moment is zero, which corresponds to the position of the single vortex modelling the lift. In the present study this point is assumed to be at the turntable centre.

From the above expression, it is seen that the $\Delta C_p/C_l$ distribution should collapse to a single curve. Additionally, it is seen that the relative error committed when using a fixed finite streamwise portion of the walls, is expected to be independent of the lift.

When using the pressures on the side walls for the C_l calculation it is in principle necessary to use the pressures infinitely upstream and downstream of the model. This is of course not possible in a wind tunnel where the side wall pressures are measured on strips with a limited length. Therefore, it is necessary to estimate the fraction of the lift not captured by the wall pressure strips. The fraction can be found by integrating the above expression over the extent of the wall pressure strip on the side walls:

$$\eta = \frac{C_{l,reduced}}{C_l} = \frac{c}{H}\int_{x_{min}}^{x_{max}} \frac{1}{\cosh\left(\pi\frac{x}{H}\right)}\mathrm{d}x \tag{2}$$

2.4. Previous wind tunnel measurements

The measurements from the PLCT and CFD simulations are compared to the originally performed measurements on the NACA63-418 [8], and previously published data from the DAN-AERO MW project [9]. In [9] measurements are presented from five different tunnels, including the data from [8]. For the present study the data from the tunnels at LM Wind Power (LM), Delft University of Technology (Delft), University of Stuttgart (Stuttgart) and the original data (Abbott) is used. Reference [9] should be consulted for details.

The data covers aspect ratios from 1.2 to 2.1, turbulence levels from 0.0002% to 0.1%, chord to tunnel height ratios from 0.22 to 0.33.

LM and Delft use pressure orifices on the model surface and Stuttgart and Abbott use tunnel wall pressures.

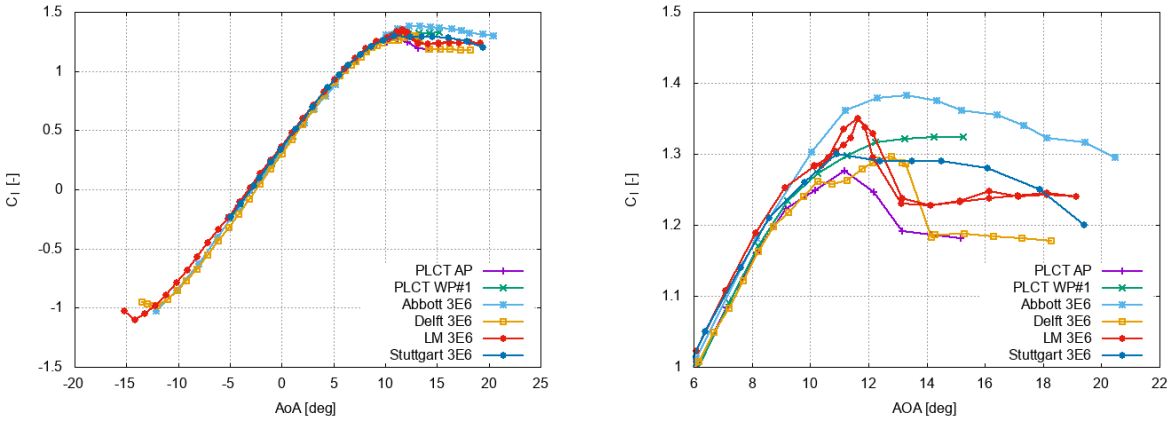

Figure 2. Lift polars (corrected) for the clean NACA63-418, Re=3E6 obtained by surface pressures (PLCT AP, Delft and LM) and wall pressures (PLCT WP#1, Abbott and Stuttgart). Right figure is a zoom of the curve shown in the left plot.

3. Results

Figure 2 shows the obtained lift polar for the clean NACA63-418 profile at a Reynolds number of 3E6 from the PLCT based on surface pressures and wall pressures. Results from the DAN-AERO MW project [9] from Delft, LM (both surface pressures) and Stuttgart (wall pressures) are included together with the original wall pressure based measurements (Abbott) from [8]. The figure shows as the only one data corrected for the wind tunnel walls. The corrections are made in accordance with [10].

Generally, the stall is more abrupt when using surface pressures ('PLCT AP', 'Delft' and 'LM'). The C_l based on the tunnel wall pressures has a smoother course around maximum C_l. Additionally, for the AoAs tested, the tunnel wall C_l is higher than the airfoil surface C_l in the stalled region.

Figure 3 and Figure 4 show lift polars for a case with vortex generators (VGs) and a tripped flow by zig-zag-tape (zz-tape), respectively. Similar trends as for the clean case is seen. For both cases it can be expected that the tunnel wall pressures show higher lift values as the effect of both VGs and zz-tape is to some degree 3D. Therefore it is probably better predicted by the tunnel wall pressures due to the spanwise averaging, than by the surface pressures, as they measure a random value of the spanwise minimum and maximum pressure. VGs are obviously more 3D than zz-tape.

The predicted maximum C_l and behavior after maximum C_l is not identical between the tunnels, however there is a general trend in the measurements: C_l measured by airfoil pressures ('PLCT AP', 'Delft' and 'LM') show a more abrupt stall characteristic with a sudden drop in C_l after maximum C_l, whereas C_l measured by side wall pressures ('PLCT WP#1', 'Abbott' and 'Stuttgart') has a more smooth stall characteristic. Since the results show similar trends, the difference is not just an effect related to the PLCT.

In [9] it was concluded that the differences in the measurements (which is not only related to maximum C_l) can be linked to differences in the airfoil model shapes, the data analysis and the calibrations. It can probably also be linked to the differences in the aspect ratio of the models, the different turbulence levels in the tunnels and the different blockage ratios (chord and thickness relative to the tunnel width).

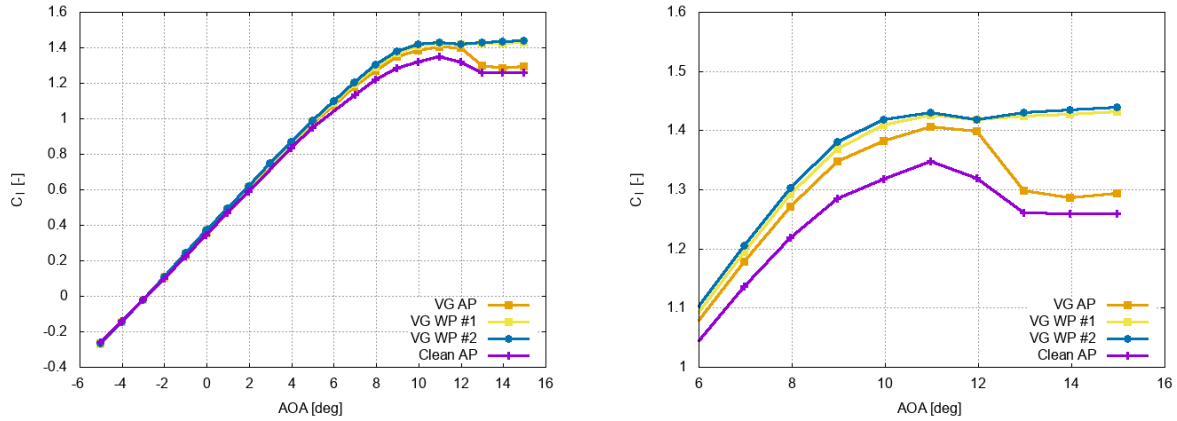

Figure 3. Lift polars (uncorrected) for the clean NACA63-418 with VGs (0.25%c high) at 60%c on the suction side, Re=3E6 obtained by surface pressures (PLCT AP) and wall pressures (PLCT WP#1). Right figure is a zoom of the curve shown in the left plot. The clean uncorected polar is shown for reference.

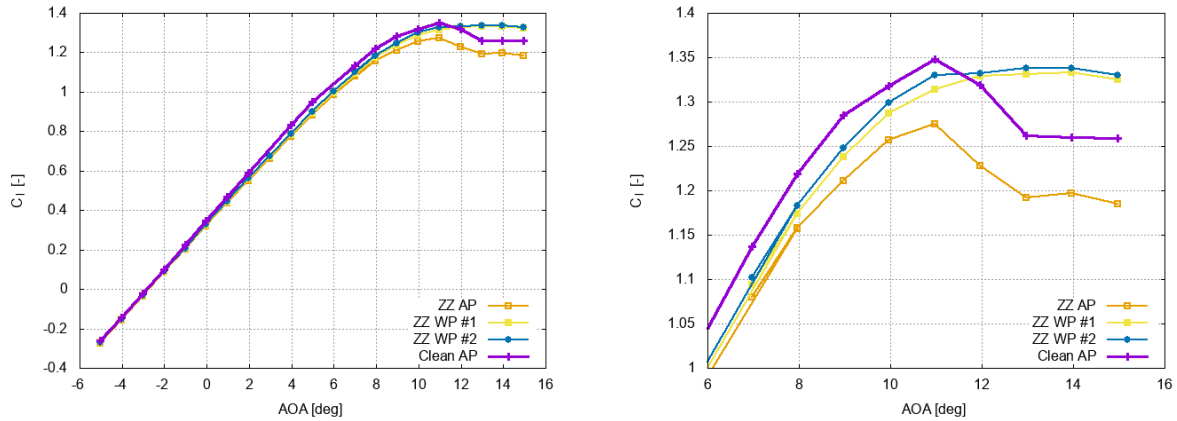

Figure 4. Lift polars (uncorrected) for the tripped (0.4mm zz-tape at 2%c suction side and 10%c pressure side) NACA63-418, Re=3E6 obtained by surface pressures (ZZ AP) and wall pressures (ZZ WP#1 and ZZ WP#2). Right figure is a zoom of the curve shown in the left plot. The clean uncorected polar is shown for reference.

In addition to the conclusions in [9] it can be mentioned that the measurements are acquired on different equipment and with a time span of almost 90 years, from the NACA measurements in the 1930s to the present 2020 PCLT measurements. This probably also influences the agreements between the obtained data.

3.1. CFD and PLCT comparisons

The 3D CFD simulations are shown in Figure 5 together with the PLCT measurements. Until the onset of separation at an AoA of 9 deg., the agreement between measurements and CFD results is very good. Thereafter the CFD simulations predicts a considerable higher maximum C_l, as is usually the case for RANS simulations. The predicted C_l from the wall pressures are also shown in the figure for AoA 8, 16 and 24 deg.

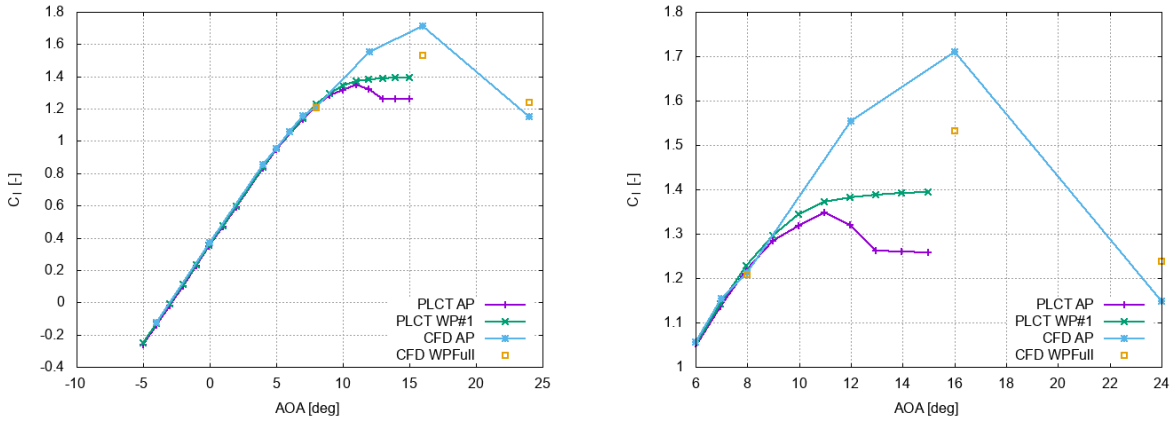

Figure 5. Lift polars (uncorrected) for the clean NACA63-418, Re=3E6 from wind tunnel measurements (PLCT) and CFD simulations. The C_l is based on airfoil pressures (AP) and wall pressures (WP). Right figure is a zoom of the curve shown in the left plot.

For AoA 8 and 16 deg. the lift from the CFD tunnel wall pressures (evaluated at 0.45m from midspan) are lower than from the CFD airfoil surface pressures evaluated at midspan. The lower lift at 8 deg. is more in-line with the expectations, since the pressures at the walls is an averaging of the pressures on the entire span of the model. The lift decreases towards the ends of the model, and therefore the average value should be lower than the C_l based on the surface pressures staggered around midspan. An example of the spanwise variation of the C_l based on surface pressures and wall pressures in the CFD simulations for 4 deg. AoA are shown in Figure 6. It is seen that the spanwise variation of C_l based on tunnel wall pressures is constant along the span whereas the C_l based on airfoil surface pressures varies along the span and, as expected, drops off at the ends, due to the end plate effects and the boundary layer at the end walls. It is also seen that the C_l at midspan is higher than the wall pressure C_l, showing that the wall pressure C_l is indeed an average of the C_l on the airfoil model.

After maximum lift the situation is more complex as the flow becomes highly 3D. The fact that the C_l from the tunnel wall pressures is higher in the stalled region suggests that the flow at the ends of the model is not as separated as on the midspan region. The small tuft survey (Figure 10) supports this, as it is obvious that the flow at midspan is more separated.

The CFD simulation at 16 deg. show a lower lift from the tunnel wall pressures than from the airfoil pressures. This is probably because the CFD simulations not necessary capture the effects of the stall cells as the RANSE CFD suppresses them and the grid is too coarse to resolve the unsteady flow phenomena at midspan. Hence, the CFD simulation still drops off at the ends even in stall.

At 24 deg. the C_l predicted by CFD based on the tunnel wall pressures are higher than the C_l predicted from airfoil surface pressure, remembering that RANS CFD in these conditions are inherent inaccurate.

The above results clearly indicate that care should be taken when using maximum C_l and C_l from the stalled region based on airfoil surface pressures, as they are highly dependent on the spanwise location of the pressures orifices relative to the 3D flow structures. On the other hand it is also questionable if C_l based on the side wall pressures is still applicable. Even though they represent an integrated value of the forces on the entire span, they probably depends on the aspect ratio of the flow and thereby are model and tunnel dependent.

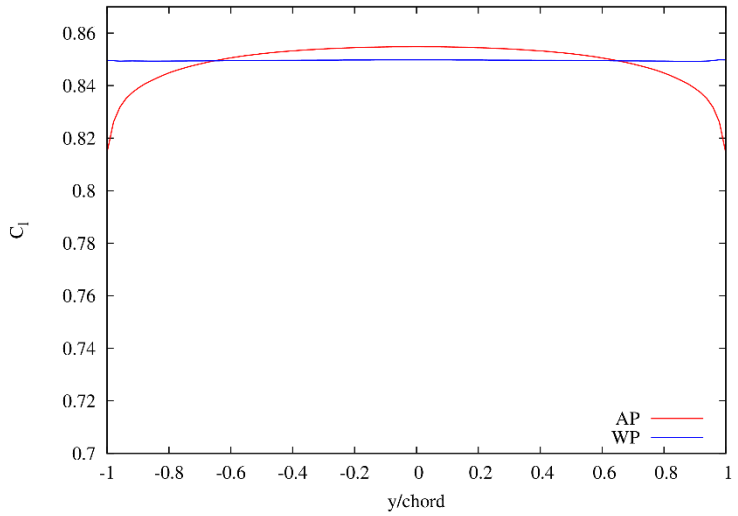

Figure 6. Spanwise Cl distributions from 3D CFD simulations, Reynolds number of 3E6 and AoA = 4 deg. Airfoil pressures is 'AP' and wall pressures are 'WP'

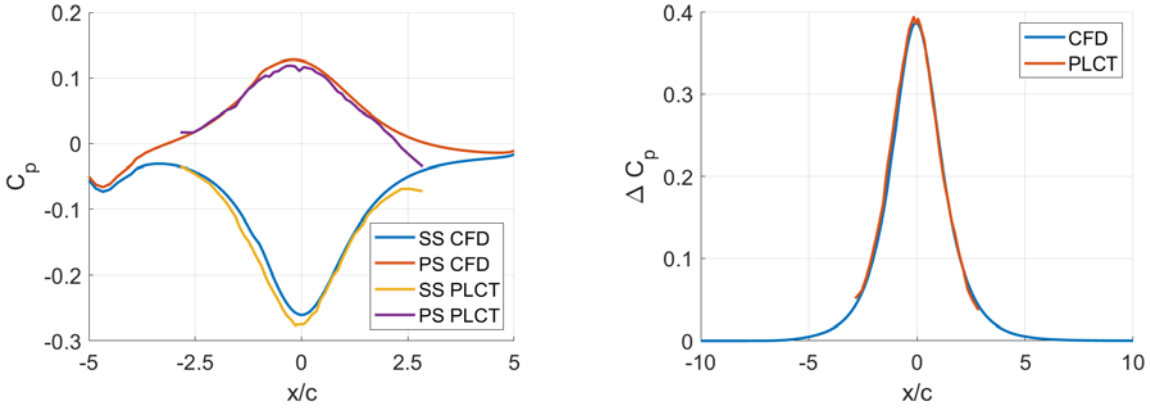

Figure 7. Wall pressure footprint 8 deg.

Figure 7 shows the wall pressure footprint at 8 deg. AoA from the CFD simulations and the PLCT measurements. The CFD C_p levels has been shifted by a constant to match the PLCT level at the pressure side (PS) at x/c = -2.55. It is seen that generally there is a good agreement between the CFD and measurements. The absolute levels of the measurements is slightly lower and the downstream tail part is somewhat skewed towards lower levels. This is a general tendency in the measurements and is believed to be caused by the influence of the wake rake support structure. However, looking at the difference in the C_p on the walls, ΔC_p (i.e. the pressure side (PS) C_p subtracted the suction side (SS) C_p), which is a measure of the lift, the agreement between CFD and measurements is very good, as seen in the right part of the figure.

Figure 8 shows that wall pressure footprint from CFD at 24 deg. AoA. The pressure are shown on the entire simulation domain, i.e. form the contraction inlet to the diffusor outlet. It is seen that the shape differ from the shape at 8 deg. and that the pressures on the opposite tunnel walls are identical except around the airfoil model.

Figure 9 shows the $\Delta C_p/C_l$ for the three CFD simulations (8, 16, and 24 deg.) and three measurements (8, 10 and 15 deg.) together with the theoretical curve from Equation (1). It is seen that the wall pressure footprint for the PLCT 8 deg., 10 deg. and 15 deg. and the CFD 8 deg. and 16 deg. almost collapses into one curve. All five curves have slightly lower peak values than predicted by

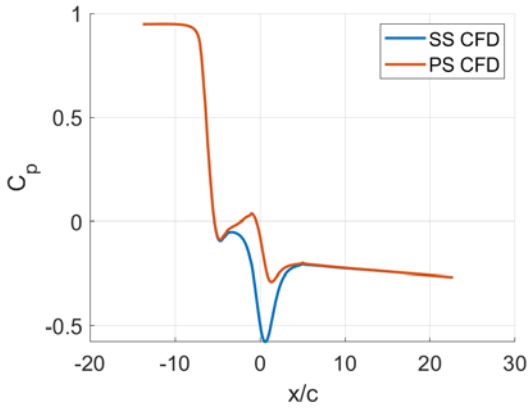

Figure 8. Wall pressure footprint from CFD at 24 deg.

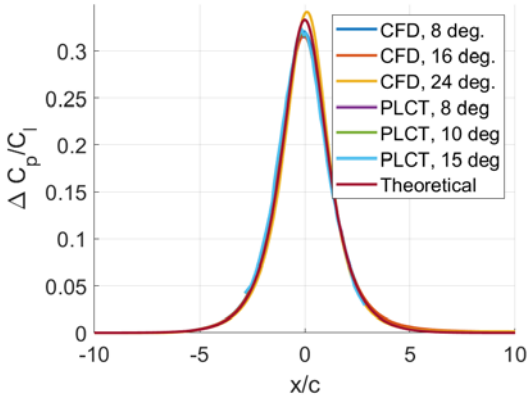

Figure 9. Wall pressure footprint from the PLCT and CFD for the NACA63-418, Re=3E6. Also shown is the theoretical distribution from Eq. (1).

Equation (1). This may be explained by the fact that the derivation of the theoretical expression is based on the aerodynamic loading acting in a single point in the tunnel, thus it does not reflect the detailed chordwise loading along the chord of the airfoil. The CFD prediction at 24 deg. differ from the ones at lower angles of attack by having a larger peak value and the downstream tail decreases steeper than the theoretical distribution.
However, the results indicates that the wall pressures can be used also for separated flow, even though the potential theory with the single vortex cannot model separation.

The CFD simulations are used to check the validity of Equation (2). Table 1 gives the fraction (η) of the C_l from the limited wall pressure strip relative to the full strip for the CFD simulations and Equation (2). It is seen that the η is a few per cent lower for the CFD simulations compared to the one applied on the PLCT measurements, however, the differences are considered to be so small that the applied method can be used.

Table 1. Fraction of the C_l captured by the wall pressure strip relative to the full strip.

	η
PLCT	0.9357
CFD, 8 deg.	0.9281
CFD, 16 deg.	0.9133
CFD, 24 deg.	0.9284

3.1.1. Tufts

In order to check the three dimensionality of the flow and investigate if the differences in the C_l after maximum C_l is caused by an inexpedient placement of the pressure orifices on the model relative to the separation line and stall cells, tuft are applied at the 70%c and 90%c, see Figure 10. The figure show pictures and pressure distributions from the pressure orifices for 5 deg., 10deg. and 15 deg.

In addition to the pictures videos where recorded in order to get a better insight of the tuft motions. The videos revealed that the flow is always attached on the PS and on the SS for 5 deg. At 5 deg. the difference in predicted C_l from the wall pressures and surface pressures is less than 0.5%.

At 10 deg. separation is seen on the last row of tufts, but the tufts at 70%c still indicates attached flow, this is also confirmed by the pressure distribution. The difference between airfoil pressure and wall pressure C_l is approximately 2%.

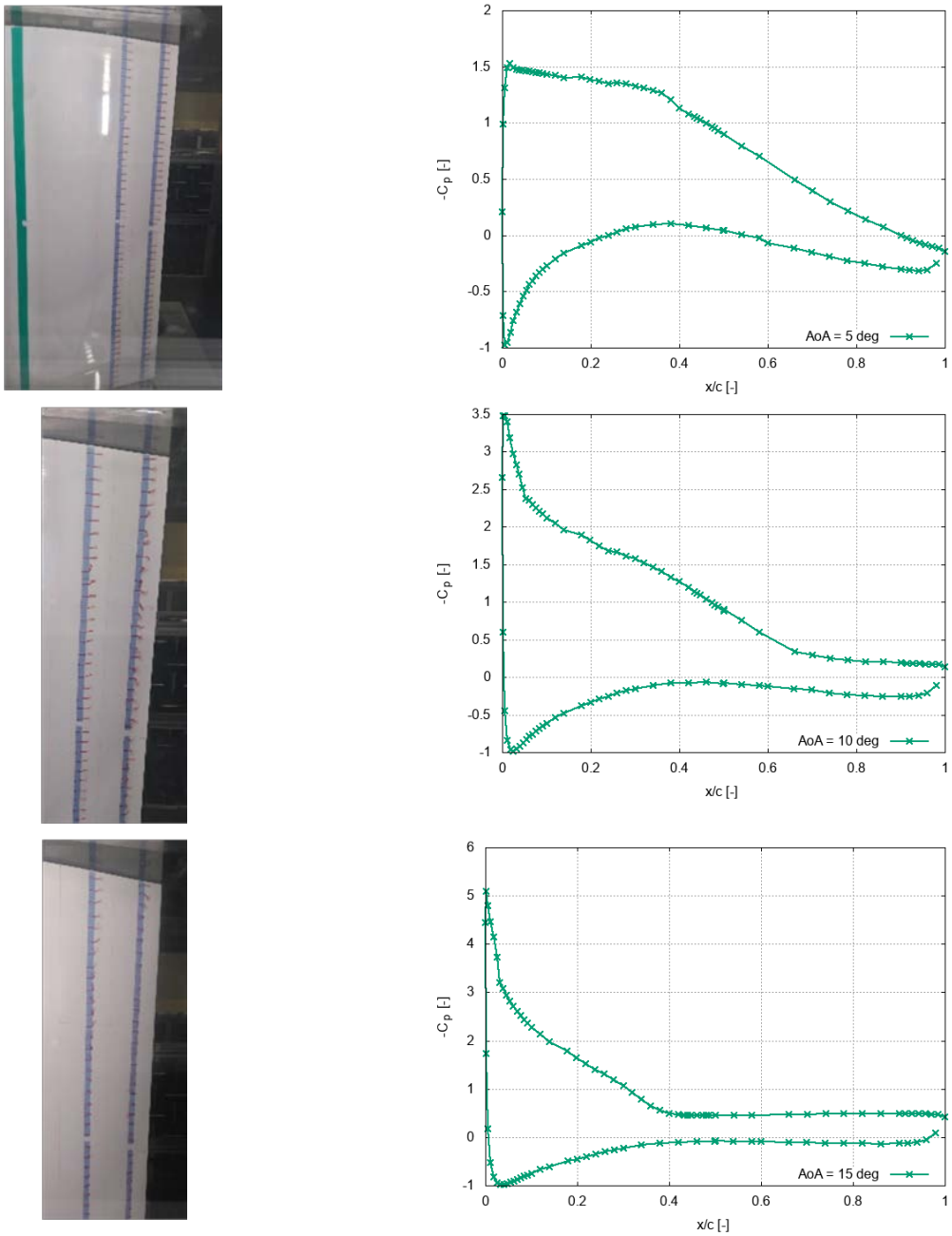

Figure 10. Tuft pictures (tufts at 70%c and 90%c) and Cp distributions. Clean, Re=3E6. Left 5 deg, middle 10 deg, right 15 deg. Flow from left to right.

At 15 deg. both rows of tufts show flow separation and the pressure distribution indicates a TE separation from 40%c. The difference in predicted C_l has now increased to more than 10%. Based on the limited amount of tufts it is difficult to see if there are stall cells present or if the tufts are only influenced by a 2D separation vortex. There is clearly a vortex structure that pushes the tufts upstream. On top of that the tufts at both end walls is still mainly in the onset flow direction, indicating a clockwise rotating vortex perpendicular to the model surface at the lower end wall and a counter-clockwise rotating vortex at the upper end wall. At midspan the tufts looks to be going almost entirely upstream, which could suggest that at the midspan section of the model the flow is more separated than at the remaining part of the model.

However, the motion of the other tufts doesn't fully suggest that there are two counter rotating vortices close to the end-walls, but perhaps the 2D separation vortex is superposed with more stall cell vortices originating perpendicular to the model surface. Looking at the tufts the entire aft part of the model looks severely separated. If the separation pattern is wedge shaped it can partly explain the 10% higher lift from the side wall pressures. However, more tufts should have been applied to get a better resolution of the separation pattern.

4. Conclusions

The CFD simulations show that when the flow is attached the lift based on the side wall pressures results in almost the same lift as calculated from the surface pressures. For attached flow the lift based on the side wall pressures should generally be lower than the lift based on the surface pressures, at least for the surface pressures around midspan. This is because the spanwise lift distribution drops off at the end walls due to the end plate effects and the boundary layer on the wall, as the side wall pressures are an averaging of the spanwise surface pressures they will be lower than the surface pressures giving a lower lift.

Around the maximum lift and in the stalled region the flow is not anymore 2D and the differences in the lift based on surface pressures and side wall pressures depend on the location of the surface pressure orifices relative to the spanwise varying separation line. For the NACA63-418 airfoil used in the present study the lift based on the side wall pressures are generally highest.

The CFD simulations confirm that the method used to predict the lift from the limited side wall pressure strips in the wind tunnel is applicable.

No clear stall cells was identified with the tufts. However, only two rows of tufts were used, so a new campaign is planned with additional rows in order to better identify the 3D structures in the stalled region.

Acknowledgements

The present study is partly funded by the EUDP project Accelerate and increase quality in aerodynamic and aeroacoustic design loops (AeroLoop), Journal nr.: 64018-0144.

References

[1] Manolesos M, Papadakis G and Voutsinas SG 2014 Experimental and computational analysis of stall cells on rectangular wings. *Wind Energy* **17**:939–55

[2] Manolesos M and Voutsinas SG 2014 Geometrical characterization of stall cells on rectangular wings. *Wind Energy* **17**:1301–14

[3] Michelsen JA, Basis3D - a Platform for Development of Multiblock PDE Solvers, AFM 92-05, Department of Fluid Mechanics, Technical University of Denmark, December 1994

[4] Michelsen JA, Block structured Multigrid solution of 2D and 3D Elliptic PDEs, AFM 94-06, Department of Fluid Mechanics, Technical University of Denmark, May 1994

[5] Sørensen, NN, General Purpose Flow Solver Applied to Flow Over Hills, Risø-R-827, Risø National Laboratory, Roskilde, Denmark, 1995

[6] Sørensen NN, Olsen AS, Bak C, Gaunaa M, Beckerlee JS, Fischer A, Mikkelsen RF and Ildvedsen S 2020 CFD modeling of the Poul la Cour Tunnel submitted to *TORQUE 2020*

[7] Althaus, D, Measurement of Lift and Drag in the Laminar Wind Tunnel, https://www.iag.uni-stuttgart.de/dateien/pdf/laminarwindkanal_messtechniken/althaus_2.pdf accessed 13 Dec. 2019

[8] Abbott IH, von Doenhoff AE. Theory of Wing Sections: Including a Summary of Airfoil data. New York: Dover Publications, Inc.; 1959.

[9] Bak C, Aagaard Madsen H, Gaunaa M, Schmidt Paulsen U, Fuglsang P, Romblad J, Olesen NA, Enevoldsen P, Laursen J and Jensen L 2010 DAN-AERO MW: Comparisons of airfoil characteristics for two airfoils tested in three different wind tunnels. in Torque 2010: The science of making torque from wind. European Wind Energy Association (EWEA), pp. 59-

70, Torque 2010, Heraklion, Greece, 28/06/2010.
[10] Allen JH and Vincenti GW 1944 Wall Interference in a Two-Dimensioanl-Flow Wind Tunnel, With Consideration of the Effect of Compressibility, NACA-TR-782